

ADER Finite Volume Schemes for Nonlinear Diffusion-Reaction Equations

Eleuterio. F. Toro (1) and Arturo Hidalgo (2)

(1) Laboratory of Applied Mathematics
Department of Civil and Environmental Engineering
University of Trento
Trento, Italy

E-mail: toro@ing.unitn.it

Website: <http://www.ing.unitn.it/toro>

(2) Departamento de Matemática Aplicada y Métodos Informáticos
ETS Ingenieros de Minas
Universidad Politécnica de Madrid
Madrid, Spain

E-mail: arturo.hidalgo@upm.es

Abstract. We construct finite volume schemes of arbitrary order of accuracy in space and time for solving nonlinear diffusion-reaction partial differential equations. The numerical schemes, written in conservative form, result from extending the Godunov and the ADER frameworks, both originally developed for approximating solutions to hyperbolic equations. The task is to define *numerical fluxes* and *numerical sources*. In the ADER approach, numerical fluxes are computed from solutions to the Derivative Riemann Problem (DRP) (or generalized Riemann problem, or high-order Riemann problem), the Cauchy problem in which the initial conditions either side of the interface are smooth functions, polynomials of arbitrary degree, for example. We propose, and systematically assess, a general DRP solver for non-linear diffusion-reaction equations and construct corresponding finite volume schemes of arbitrary order of accuracy. Schemes of 1st to 10-th order of accuracy in space and time are implemented and systematically assessed, with particular attention to their convergence rates. Numerical examples are also given.

Key words: Diffusion, Source Terms, Finite Volumes, Godunov's method, Derivative Riemann Problem, ADER, Arbitrary Accuracy.

1 Introduction

This paper deals with the construction of numerical schemes for solving nonlinear diffusion-reaction partial differential equations. These arise in a large variety of application areas, such as flow in porous media; here several processes may take place, such as solute transport by diffusion-dispersion-reaction mechanisms or heat transfer by conduction. Examples of relevant works on the mathematical formulation of these problems are [11, 30, 31, 41, 44, 43]. A particularly interesting case in porous media flow is the well-known Richards' equation, formulated by Lorenzo A. Richards in 1931, which represents groundwater flow in the unsaturated zone. See for example [5, 7, 16, 23]. Many other physico-chemical processes can be modelled by means of nonlinear diffusion-reaction equations, such as heat conduction in plasma [8, 9, 45], combustion problems [4, 24, 47], liquid evaporation [29], population genetics [4, 28] and, of more recent interest, image processing [22, 27], to name but a few. A great effort is being made in the development of the mathematical theory of nonlinear diffusion equations and to obtain exact solutions for special cases. Some results can be found in [11, 30, 31, 43, 44].

Numerical methods for diffusion-reaction equations to obtain approximate solutions is also a very active area nowadays. Finite element methods are probably the dominant numerical approach to solve these parabolic equations. Their accuracy and mesh flexibility are two of their main attractions. See for example [1, 2, 7, 14, 15], to quote but a few. Other numerical approaches for parabolic equations include finite difference methods and finite volume methods [16, 21, 22, 26, 27]. Discontinuous Galerkin (DG) finite element methods are also being developed to solve these parabolic equations [18, 32, 42]. For hyperbolic equations it is the class of finite volume schemes of the Godunov-type the one that dominates nowadays, with a visible increase in the popularity of DG methods. Most of the current finite volume methods make use of the Riemann problem as the building block [39], [25], a tendency that is also seen for DG methods. Two related, but distinct, works are those of Titarev and Toro [35] and Gassner et al. [18]. In the former, the authors studied ADER finite volume schemes for the linear advection-diffusion equation using a simple DRP solver. In the latter, the authors also adopted the ADER approach but in the frame of DG finite element methods; they constructed high-order methods for the diffusion equation.

In this paper we set out to construct Godunov-type finite volume schemes for non-linear diffusion-reaction equations. The classical Godunov method is understood as that in which one uses the solution of the Riemann problem with piece-wise constant data, which we call here the *classical* Riemann problem. In our first attempt using local solutions of classical Riemann problem we found the Godunov approach to be too restrictive: a consistent scheme is found only for a particular choice of the time step, effectively. A re-interpretation of the Godunov approach, still using solutions of classical Riemann problems, following the WAF framework [36], [10] is more productive. The well-known FTCS (Forward in Time Central in Space) finite difference scheme is reproduced, in a finite volume setting.

Another way of constructing useful finite volume schemes of the Godunov type for diffusion-reaction equations is provided by the ADER approach [40]. This is the main part of this paper. The basic ingredient of the ADER approach is the so called Derivative Riemann Problem. This is the Cauchy problem for the relevant PDEs with initial conditions consisting of piece-wise smooth data, rather than piece-wise constant as for the classical Riemann problem. The simplest case of piece-wise linear data reproduces the so called generalized Riemann problem, or GRP [6]. A particular data reconstruction with slopes obtained by central differences yields a useful Godunov scheme for the diffusion equation. It is consistent and conditionally stable, with stability limit of 2, which is four times that of the classical FTCS scheme. Thus a basic ingredient of useful finite volume Godunov-type schemes for diffusion is *data reconstruction*, as for the well-established high order schemes for hyperbolic equations. As a consequence, one is also led to the construction of schemes of high order of accuracy. In this paper we use ENO (essentially non-oscillatory) reconstructions. For background on the ADER approach for hyperbolic problems see for example [40], [33], [37], [38], [13]. In this paper, we extend the technique proposed in [37, 38], to solve the DRP for non-linear diffusion-reaction equations. The DRP solvers are systematically assessed against exact solutions. Use of these local DRP solutions leads to finite volume numerical schemes of arbitrary order of accuracy in both space and time and for the coupled diffusion-reaction processes. The schemes are systematically assessed, with particular attention paid to a detailed study of convergence rates. Methods of up to 10-th order of accuracy in space and time are developed, implemented and assessed.

The rest of this paper is structured as follows: in section 2 we discuss some mathematical and numerical preliminaries regarding finite volume schemes for diffusion-reaction equations, the Riemann problem and related Godunov methods. In section 3 we pose and solve the Derivative Riemann Problem for non-linear diffusion-reaction equations. In section 4 we assess the approximate solvers for the DRP against reference solutions. In section 5 we construct ADER numerical methods for diffusion-reaction equations. In section 6 we study the convergence rates of the schemes. In section 7 we present some numerical examples, while conclusions are drawn

in section 8.

2 Preliminaries

We construct high-order finite volume schemes for the class of diffusion-reaction equations

$$\partial_t q(x, t) = \partial_x(\alpha(x, t, q(x, t))\partial_x q(x, t)) + s(x, t, q(x, t)), \quad (1)$$

in which $q(x, t)$ is the dependent variable (unknown); x, t are the spatial and temporal independent variables; $\alpha(x, t, q(x, t))$ is a prescribed function, the diffusion coefficient; and $s(x, t, q(x, t))$ is a source (or forcing, or reaction) term. We allow for explicit dependency of the functions α and s on the independent variables x and t , although for convenience, in the rest of this paper shall often omit their explicit presence. The linear version of (1) with constant coefficients is

$$\partial_t q = \hat{\alpha}\partial_x^{(2)}q + \beta q, \quad (2)$$

where $\hat{\alpha}$ is a constant diffusion coefficient and β is a constant reaction coefficient of dimensions reciprocal of time. This model diffusion-reaction equation will be extensively used in developing and testing ideas regarding numerical methods for the more general case (1).

2.1 The Finite Volume Framework

To start with, we consider the control volume $V = [x_{i-\frac{1}{2}}, x_{i+\frac{1}{2}}] \times [t^n, t^{n+1}]$ in the $x-t$ half-plane, of dimensions

$$\Delta x = x_{i+\frac{1}{2}} - x_{i-\frac{1}{2}}, \quad \Delta t = t^{n+1} - t^n. \quad (3)$$

Integration of equation (1) in space and time in the control volume V yields the *exact relation*

$$q_i^{n+1} = q_i^n + \frac{\Delta t}{\Delta x}[g_{i+\frac{1}{2}} - g_{i-\frac{1}{2}}] + \Delta t s_i, \quad (4)$$

where

$$q_i^n = \frac{1}{\Delta x} \int_{x_{i-\frac{1}{2}}}^{x_{i+\frac{1}{2}}} q(x, t^n) dx, \quad (5)$$

is the spatial integral average of q at time t^n ,

$$g_{i+\frac{1}{2}} = -\frac{1}{\Delta t} \int_0^{\Delta t} \alpha(q(x_{i+\frac{1}{2}}, t))\partial_x q(x_{i+\frac{1}{2}}, t) dt \quad (6)$$

is the temporal integral average at the interface $x = x_{i+1/2}$, and

$$s_i = \frac{1}{\Delta x \Delta t} \int_{x_{i-\frac{1}{2}}}^{x_{i+\frac{1}{2}}} \int_{t^n}^{t^{n+1}} s(q(x, t)) dx dt \quad (7)$$

is the volume integral of the source term.

Finite volume schemes of the form (4) to solve (1) can be constructed by specifying approximations $\tilde{g}_{i+\frac{1}{2}}$ and \tilde{s}_i to $g_{i+\frac{1}{2}}$ and s_i in (6) and (7), which allow the updating of the approximate cell average \tilde{q}_i^n to the new approximate cell average \tilde{q}_i^{n+1} . By dropping the tildes we can interpret (4) as a one-step finite volume numerical scheme to solve (1) approximately. Strictly speaking the averages $\{q_i^0\}$ should be evaluated by exact integration of the appropriate initial conditions, as in (5). We call $g_{i+\frac{1}{2}}$ the *numerical flux* and s_i the *numerical source* of the finite volume scheme. In this numerical context Δx is the volume or length of the *cell*, $x_{i-\frac{1}{2}}$ and $x_{i+\frac{1}{2}}$ are the cell interfaces, $x_i = \frac{1}{2}(x_{i-\frac{1}{2}} + x_{i+\frac{1}{2}})$ is the cell centre and Δt is the time step.

In constructing approximate fluxes $g_{i+1/2}$ and approximate sources s_i , it is convenient to interpret (5)-(7) in local coordinates, with x representing $x - x_{i+1/2}$ and t representing $t - t^n$, so that the interface $x_{i+1/2}$ is located at 0 and t^n corresponds to 0.

2.2 The Riemann Problem and Godunov-type Methods

One may speculate as to whether the Godunov approach [19] might be productive in constructing finite volume schemes for diffusion equations. Here we discuss the Riemann problem, numerical fluxes and related numerical methods.

2.2.1 The Classical Riemann Problem

The *classical* (in the sense of having piece-wise constant data) Riemann problem is the Cauchy problem

$$\left. \begin{aligned} \partial_t q &= \hat{\alpha} \partial_x^{(2)} q, \quad -\infty < x < \infty, t > 0, \\ q(x, 0) &= \begin{cases} q_L & \text{if } x < 0, \\ q_R & \text{if } x > 0, \end{cases} \end{aligned} \right\} \quad (8)$$

where x and t denote local coordinates; $x = 0$ corresponds to the interface and $t = 0$ corresponds to the global time t^n (time level n). Fig. 1a depicts the piece-wise constant initial conditions, with a discontinuity at the origin. Fig. 1b shows profiles $q(x, t_k), k = 1, 2, 3$ of the solution of the Riemann problem at times $0 < t_1 < t_2 < t_3$, the solution is smooth for $t > 0$. Fig. 1c shows a contour plot of the solution $q(x, t)$ in the vicinity of the origin. For the linear equation (2) it is possible to obtain the solution of the Riemann problem (8) analytically, as seen below.

Proposition 1: The exact solution of the classical Riemann problem (8) is

$$q(x, t) = \frac{1}{2}(q_L + q_R) + \frac{1}{2}(q_R - q_L) \operatorname{erf} \left(\frac{x}{2\sqrt{\hat{\alpha}t}} \right), \quad t > 0. \quad (9)$$

Proof: As well known (see for example [46]) the solution of problem (8) can be expressed as

$$q(x, t) = \frac{q_L}{2\sqrt{\hat{\alpha}\pi t}} \int_{-\infty}^0 e^{-\frac{(x-\xi)^2}{4\hat{\alpha}t}} d\xi + \frac{q_R}{2\sqrt{\hat{\alpha}\pi t}} \int_0^{\infty} e^{-\frac{(x-\xi)^2}{4\hat{\alpha}t}} d\xi. \quad (10)$$

Using the substitution $\eta = \frac{x-\xi}{2\sqrt{\hat{\alpha}t}}$ we have $d\eta = -\frac{d\xi}{2\sqrt{\hat{\alpha}t}}$, from which

$$q(x, t) = \frac{q_L}{\sqrt{\pi}} \int_{\frac{x}{2\sqrt{\hat{\alpha}t}}}^{\infty} e^{-\eta^2} d\eta + \frac{q_R}{\sqrt{\pi}} \int_{-\infty}^{\frac{x}{2\sqrt{\hat{\alpha}t}}} e^{-\eta^2} d\eta. \quad (11)$$

We rearrange (11) as

$$q(x, t) = \frac{q_L}{\sqrt{\pi}} \left[\int_0^{\infty} e^{-\eta^2} d\eta - \int_0^{\frac{x}{2\sqrt{\hat{\alpha}t}}} e^{-\eta^2} d\eta \right] + \frac{q_R}{\sqrt{\pi}} \left[\int_{-\infty}^0 e^{-\eta^2} d\eta + \int_0^{\frac{x}{2\sqrt{\hat{\alpha}t}}} e^{-\eta^2} d\eta \right], \quad (12)$$

where

$$\int_0^{\infty} e^{-\eta^2} d\eta = \int_{-\infty}^0 e^{-\eta^2} d\eta = \frac{\sqrt{\pi}}{2}. \quad (13)$$

From (12) and (13) it follows

$$q(x, t) = \frac{q_L + q_R}{2} + \frac{q_R - q_L}{\sqrt{\pi}} \int_0^{\frac{x}{2\sqrt{\hat{\alpha}t}}} e^{-\eta^2} d\eta, \quad (14)$$

which reproduces the sought expression (10), as claimed.

Corollary 1: The spatial gradient of the solution (9) of the *classical* Riemann problem (8) is given by

$$\partial_x q(x, t) = \frac{q_R - q_L}{2\sqrt{\hat{\alpha}\pi t}} e^{-\frac{x^2}{4\hat{\alpha}t}} \quad \text{for } t > 0, \quad (15)$$

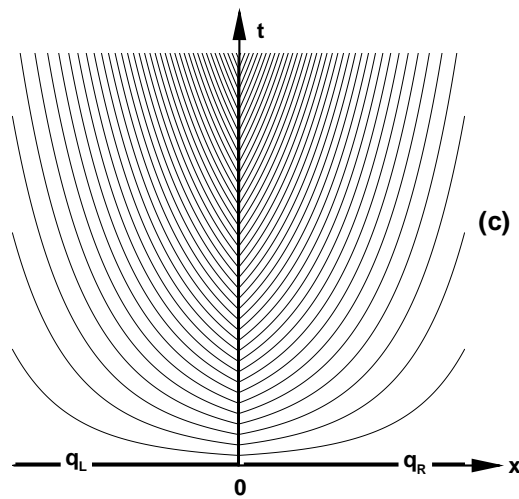
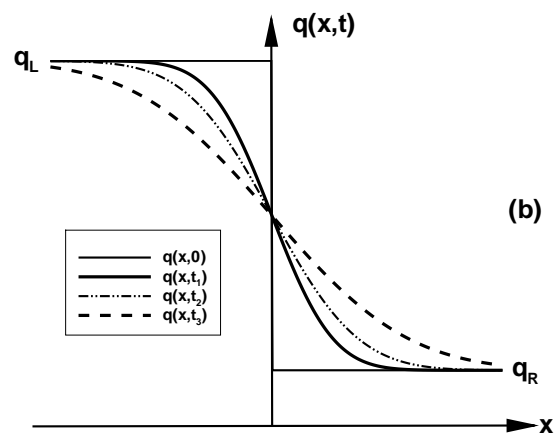
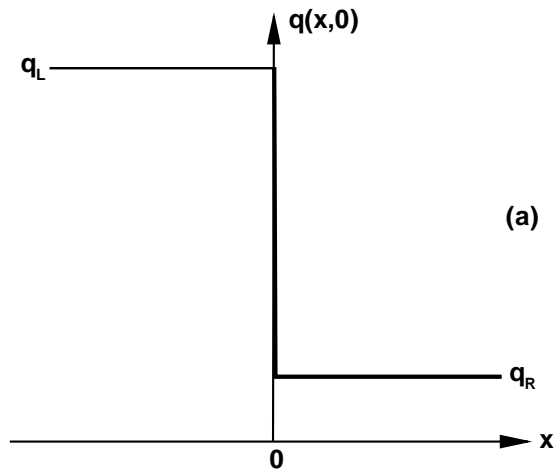


Figure 1: The classical Riemann problem for the homogeneous version of the model diffusion equation (2).

the solution at the interface is

$$q(0, t) = \frac{1}{2}(q_L + q_R) \quad \text{for } t > 0 \quad (16)$$

and the limiting value at the interface, as time tends to zero from above, is obviously given by

$$q(0, 0_+) = \lim_{t \rightarrow 0_+} q(0, t) = \frac{1}{2}(q_L + q_R) . \quad (17)$$

Proof: Omitted.

2.2.2 Godunov methods

With the exact solution of the classical Riemann problem available, it would appear entirely reasonable to attempt to construct finite volume methods of the Godunov-type by finding a numerical flux. Here we follow the WAF approach, as proposed for hyperbolic conservation laws in [36], [10], whereby numerical fluxes are sought as approximations to integrals in appropriately chosen control volumes and integrand functions. We thus search for numerical fluxes for diffusion from space-time integrals of the form

$$g_{i+\frac{1}{2}} = \frac{1}{\delta t} \frac{1}{\delta x} \int_0^{\gamma_0 \Delta t} \int_{-\gamma_L \Delta x}^{\gamma_R \Delta x} G(q(x, t), \partial_x q(x, t)) dx dt , \quad (18)$$

where $\delta x = (\gamma_L + \gamma_R)\Delta x$, $\delta t = \gamma_0 \Delta t$ and $\gamma_L, \gamma_0, \gamma_R$ are three non-negative real numbers. The integrand function $G(q(x, t), \partial_x q(x, t))$ is also open to choice.

Here we study the special case in which $\gamma_L = \gamma_R = 0$ and $G(q(x, t), \partial_x q(x, t)) = -\hat{\alpha} \partial_x q(0, t)$. Thus we have

$$g_{i+\frac{1}{2}} = -\frac{1}{\gamma_0 \Delta t} \int_0^{\gamma_0 \Delta t} \hat{\alpha} \partial_x q(0, t) dt , \quad (19)$$

which denotes a time-integral average in the time interval $[0, \gamma_0 \Delta t]$. Use of (15) into (19) gives the numerical flux

$$g_{i+\frac{1}{2}} = -\sqrt{\frac{\hat{\alpha}}{\gamma_0 \pi \Delta t}} (q_{i+1}^n - q_i^n) . \quad (20)$$

Substituting this into (4) gives the finite volume method

$$q_i^{n+1} = q_i^n + \tilde{d}(q_{i+1}^n - 2q_i^n + q_{i-1}^n) , \quad (21)$$

with definitions

$$\tilde{d} = \sqrt{\frac{d}{\gamma_0 \pi}} , \quad d = \frac{\hat{\alpha} \Delta t}{\Delta x^2} . \quad (22)$$

A linear stability analysis reveals that the scheme (21) is conditionally stable, with stability condition

$$0 \leq \tilde{d} \leq \frac{1}{2} \quad \text{or} \quad 0 \leq d \leq \frac{\gamma_0 \pi}{4} . \quad (23)$$

A consistency analysis of the scheme gives the relation

$$\partial_t q(x_i, t^n) = \hat{\alpha} \sqrt{\frac{1}{\gamma_0 \pi d}} \partial_x^{(2)} q(x_i, t^n) + \mathcal{O}(\Delta t) + \mathcal{O}(\Delta x^2) , \quad (24)$$

implying the following constraint $\gamma_0 = \frac{1}{\pi d}$, which in turn determines the integration interval as $[0, \frac{\Delta t}{\pi d}]$.

Remarks:

- The Godunov approach for diffusion, interpreted in the WAF sense, reproduces identically the well-known FTCS (Forward in Time Central in Space) finite difference scheme but interpreted as a finite volume method,

$$q_i^{n+1} = q_i^n + d(q_{i+1}^n - 2q_i^n + q_{i-1}^n), \quad (25)$$

with numerical flux

$$g_{i+\frac{1}{2}}^{FTCS} = -\hat{\alpha} \frac{q_{i+1}^n - q_i^n}{\Delta x}. \quad (26)$$

- Had we taken $\gamma_0 = 1$, as done in the classical Godunov method, we would have obtained one very particular useful scheme, namely the FTCS scheme as a finite volume scheme, with $d = \frac{1}{\pi}$. In other words, the classical interpretation of Godunov method for diffusion, still using the classical Riemann problem solution, is not productive, unless re-interpreted in the WAF sense.

The use of high-order Riemann problems following the ADER approach, first proposed for hyperbolic equations, provides another way, perhaps more general, for constructing finite volume methods of the Godunov type for diffusion equations. This is the main subject of this paper.

2.3 Another Godunov Method

We consider the ADER approach [40], for which the building block is the solution of the Derivative Riemann Problem, that is the Cauchy problem

$$\left. \begin{aligned} \partial_t q &= \hat{\alpha} \partial_x^{(2)} q, \quad -\infty < x < \infty, t > 0, \\ q(x, 0) &= \begin{cases} q_L(x) & \text{if } x < 0, \\ q_R(x) & \text{if } x > 0, \end{cases} \end{aligned} \right\} \quad (27)$$

where $q_L(x)$ and $q_R(x)$ are two smooth functions away from zero, with a discontinuity at the origin. In a numerical setting these functions will be polynomial functions of the desired degree resulting from a *reconstruction procedure* based on the set of cell integral averages $\{q_i^n\}$.

The simplest, still conservative, reconstruction is the first-degree polynomial

$$p_i(x) = q_i^n + (x - x_i) \Delta_i, \quad (28)$$

where Δ_i is a slope for cell i , for which an obvious choice is

$$\Delta_i = \frac{q_{i+1}^n - q_{i-1}^n}{2\Delta x}. \quad (29)$$

Returning to the question of determining a numerical flux via (6), we first need to define the spatial gradient at the interface. This is accomplished by first establishing the following elementary but useful result.

Proposition 2: The k -order spatial gradient of the solution of $q(x, t)$ of (2) obeys identically equation (2), that is

$$\partial_t(\partial_x^{(k)} q) = \hat{\alpha} \partial_x^{(2)}(\partial_x^{(k)} q) + \beta(\partial_x^{(k)} q). \quad (30)$$

Proof: Omitted.

We can therefore pose the *classical Riemann problem for derivatives*

$$\left. \begin{aligned} \partial_t(\partial_x^{(1)} q) &= \hat{\alpha} \partial_x^{(2)}(\partial_x^{(1)} q), \quad -\infty < x < \infty, t > 0, \\ \partial_x^{(1)} q(x, 0) &= \begin{cases} \Delta_i & \text{if } x < 0, \\ \Delta_{i+1} & \text{if } x > 0, \end{cases} \end{aligned} \right\} \quad (31)$$

whose solution, after (16), is

$$\partial_x^{(1)} q(0, t) = \frac{1}{2}(\Delta_i + \Delta_{i+1}) \quad \text{for } t > 0. \quad (32)$$

Evaluation of (6) gives the numerical flux

$$g_{i+\frac{1}{2}} = -\frac{\hat{\alpha}}{4\Delta x}(q_{i+1}^n + q_{i+2}^n - q_{i-1}^n - q_i^n) \quad (33)$$

and the corresponding Godunov scheme is

$$q_i^{n+1} = q_i^n + \frac{1}{4}d(q_{i+2}^n - 2q_i^n + q_{i-2}^n). \quad (34)$$

This scheme is consistent and stable, with stability condition $0 \leq d \leq 2$, whose upper limit is four times larger than that of the FTCS scheme (25).

We note that scheme (34) for the homogeneous diffusion equation (2) resembles the Lax-Friedrichs scheme for hyperbolic equations. The immediate neighbours of q_i^n do not contribute to its updating to q_i^{n+1} to the next time level.

Variations of scheme (34) can be obtained by redefining the slopes in the reconstruction. For example, we can take

$$\Delta_i = \gamma\left(\frac{q_i^n - q_{i-1}^n}{\Delta x}\right) + (1 - \gamma)\left(\frac{q_{i+1}^n - q_i^n}{\Delta x}\right), \quad 0 \leq \gamma \leq 1. \quad (35)$$

The special value $\gamma = \frac{1}{2}$ reproduces (34).

It seems as if initial value problems with non-identical vanishing gradients can lead to useful Godunov schemes for diffusion.

3 The Derivative Riemann Problem (DRP)

In this section we introduce the Derivative Riemann Problem, or DRP, for non-linear diffusion-reaction equations and study a method of solution. In a numerical context, local solutions of Derivative Riemann Problems will be used to construct numerical fluxes for high order Godunov-type methods for parabolic equations (1).

3.1 The Problem

We call the following Cauchy problem

$$\left. \begin{aligned} \partial_t q(x, t) &= \partial_x(\alpha(q(x, t))\partial_x q(x, t)) + s(x, t, q(x, t)), \quad -\infty < x < \infty, \quad t > 0, \\ q(x, 0) &= \begin{cases} q_L(x) & \text{if } x < 0, \\ q_R(x) & \text{if } x > 0, \end{cases} \end{aligned} \right\} \quad (36)$$

the Derivative Riemann Problem, where the initial condition $q(x, 0)$ consists of two arbitrary functions $q_L(x)$ and $q_R(x)$ that are smooth away from zero. Figure 2 depicts a typical distribution of the initial conditions for the IVP (36). We look for a solution $q_{LR}(\tau)$, right at the interface $x = 0$, as a function of time τ . In the spirit of the Cauchy-Kowaleswki method, see for example [46], we express the sought solution at $x = 0$ as a power series expansion in time as follows

$$q_{LR}(\tau) = q(0, 0_+) + \tau\partial_t q(0, 0_+) + \dots + \frac{\tau^k}{k!}\partial_t^{(k)} q(0, 0_+) + \mathcal{O}(\tau^{K+1}), \quad (37)$$

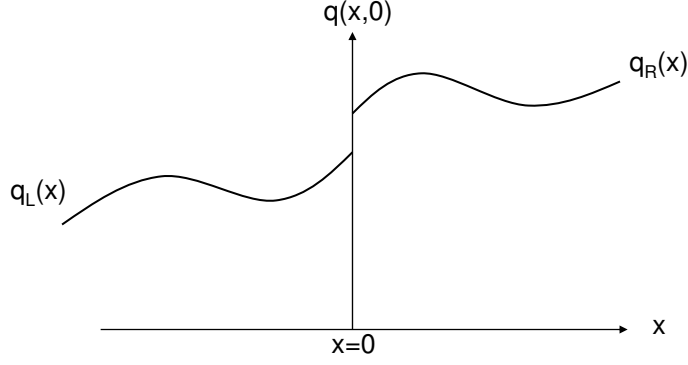


Figure 2: General initial condition for the Derivative Riemann Problem (DRP).

where

$$0_+ = \lim_{\tau \rightarrow 0} \tau, \quad \partial_t^{(k)} q(x, t) \equiv \frac{\partial^k q(x, t)}{\partial t^k}, \quad \text{for } k = 1, \dots, K. \quad (38)$$

We truncate the series by neglecting error terms $\mathcal{O}(\tau^{K+1})$ and thus obtain $K + 1$ terms in (37). If $q_L(x)$ and $q_R(x)$ are polynomials of order at most K then the truncation is justified.

To compute each term of (37), and thus to compute the complete solution, we follow the methodology put forward in [37], [38], as applied to hyperbolic equations. The technique can be applied to the complete non-linear inhomogeneous IVP (36), but for ease of exposition we consider four distinct cases: the linear homogeneous case, the linear inhomogeneous case, the non-linear homogeneous case and the nonlinear inhomogeneous case.

3.2 The Linear Homogeneous Case

We consider the linear homogeneous case with constant diffusion coefficient $\hat{\alpha}$

$$\left. \begin{aligned} \partial_t q(x, t) &= \hat{\alpha} \partial_x^{(2)} q(x, t), \quad -\infty < x < \infty, t > 0, \\ q(x, 0) &= \begin{cases} q_L(x) & \text{if } x < 0, \\ q_R(x) & \text{if } x > 0. \end{cases} \end{aligned} \right\} \quad (39)$$

The sought solution at $x = 0$ has the form (37), for which we need to determine the leading term and the coefficients of the higher order terms.

3.2.1 The leading term

The leading term $q(0, 0_+)$ in (37) accounts for the *first-instant interaction* of the initial conditions and is obtained by solving exactly the following classical (piece-wise constant data) Riemann problem

$$\left. \begin{aligned} \partial_t q(x, t) &= \hat{\alpha} \partial_x^{(2)} q(x, t), \quad -\infty < x < \infty, t > 0, \\ q(x, 0) &= \begin{cases} \lim_{x \rightarrow 0^-} q_L(x) \equiv q_L(0) & \text{if } x < 0, \\ \lim_{x \rightarrow 0^+} q_R(x) \equiv q_R(0) & \text{if } x > 0. \end{cases} \end{aligned} \right\} \quad (40)$$

Application of *Corollary 1*, equation (17), gives the exact solution as

$$q(0, 0_+) = \frac{1}{2} (q_L(0) + q_R(0)). \quad (41)$$

3.2.2 Higher order terms

The higher order terms require the calculation of the coefficients, which are the time derivatives $\partial_t^{(k)} q(0, 0_+)$. Here we apply the Cauchy-Kowalewski procedure to convert time derivatives to functions of spatial derivatives using the governing equation. It is easily seen that

$$\partial_t^{(k)} q(x, t) = \hat{\alpha}^k \partial_x^{(2k)} q(x, t), \text{ for } k = 1, \dots, K. \quad (42)$$

Therefore the sought coefficients in (37) are given by

$$\partial_t^{(k)} q(0, 0_+) = \hat{\alpha}^k \partial_x^{(2k)} q(0, 0_+), \text{ for } k = 1, \dots, K. \quad (43)$$

Now the problem consists of determining the space derivatives in (43). But for the linear equation with constant diffusion coefficient we have already shown, *Proposition 2*, that $\partial_x^{(k)} q(x, t)$ obeys the original evolution equation, see (30). We can therefore pose and solve the classical Riemann problem with piece-wise constant data for derivatives, namely

$$\left. \begin{aligned} \partial_t(\partial_x^{(2k)} q(x, t)) &= \hat{\alpha} \partial_x^{(2)} (\partial_x^{(2k)} q(x, t)), \quad -\infty < x < \infty, t > 0, \\ \partial_x^{(2k)} q(x, 0) &= \begin{cases} q_L^{(2k)}(0) \equiv \lim_{x \rightarrow 0^-} \frac{d^{2k}}{dx^{2k}} q_L(x) & \text{if } x < 0, \\ q_R^{(2k)}(0) \equiv \lim_{x \rightarrow 0^+} \frac{d^{2k}}{dx^{2k}} q_R(x) & \text{if } x > 0. \end{cases} \end{aligned} \right\} \quad (44)$$

Again, from *Corollary 1* the form of the solution to this problem is the same as that for the leading term, namely

$$\partial_x^{(2k)} q(0, 0_+) = \frac{1}{2} \left(q_L^{(2k)}(0) + q_R^{(2k)}(0) \right) \quad (45)$$

and the final solution reads

$$q_{LR}(\tau) = \sum_{k=0}^K \left[\frac{\frac{1}{2} \hat{\alpha}^k \left(q_L^{(2k)}(0) + q_R^{(2k)}(0) \right)}{k!} \right] \tau^k. \quad (46)$$

3.3 The Linear Inhomogeneous Case

The problem we consider now is the linear diffusion equation with a source term, which depends linearly on the unknown $q(x, t)$:

$$\left. \begin{aligned} \partial_t q(x, t) &= \hat{\alpha} \partial_x^{(2)} q(x, t) + \beta q(x, t), \quad -\infty < x < \infty, t > 0, \\ q(x, 0) &= \begin{cases} q_L(x) & \text{if } x < 0, \\ q_R(x) & \text{if } x > 0. \end{cases} \end{aligned} \right\} \quad (47)$$

The solution procedure is very similar to the one described for the homogeneous case. Applying the Cauchy-Kowalewski procedure, time derivatives can be expressed as

$$\partial_t^{(k)} q(x, t) = \sum_{l=0}^k \binom{k}{l} \beta^l \hat{\alpha}^{k-l} \partial_x^{(2(k-l))} q(x, t) \quad (48)$$

and the interface solution can be written in the form:

$$q_{LR}(\tau) = \frac{1}{2} (q_L(0) + q_R(0)) + \sum_{k=1}^K \frac{\tau^k}{k!} \left[\frac{1}{2} \sum_{l=0}^k \beta^l \hat{\alpha}^{k-l} \left(q_L^{2(k-l)} + q_R^{2(k-l)} \right) \right]. \quad (49)$$

3.4 The Non-linear Homogeneous Case

The problem to solve is

$$\left. \begin{aligned} \partial_t q(x, t) &= \partial_x (\alpha(q) \partial_x q(x, t)) , -\infty < x < \infty , t > 0 , \\ q(x, 0) &= \begin{cases} q_L(x) & \text{if } x < 0 , \\ q_R(x) & \text{if } x > 0 . \end{cases} \end{aligned} \right\} \quad (50)$$

Again the proposed solution has the form (37). The solution strategy is analogous to that for the linear problem, the difference being in the evaluation of the functions of space derivatives. In the linear case these functions were the linear functions (42). Now the full non-linearity of the governing equation enters the problem. In general one has

$$\partial_t^{(k)} q(x, t) = P^{(k)} \left(\partial_x^{(0)} q(x, t), \dots, \partial_x^{(2k)} q(x, t) \right) . \quad (51)$$

For example, for $k = 1$ we have

$$\partial_t q(x, t) = P^{(1)} = \alpha(q) \partial_x^{(2)} q(x, t) + \alpha'(q(x, t)) (\partial_x q(x, t))^2 . \quad (52)$$

We note that the reliable evaluation of the higher order time derivatives requires the use of algebraic manipulators. To fully determine the functions $P^{(k)}$ in (51) we need to obtain all the space derivatives of $q(x, t)$, which are the arguments of the functions. To this end we propose to solve linearized classical Riemann problems for space derivatives, as done for the linear case. The solution is given by

$$q_{LR}(\tau) = \frac{1}{2} (q_L(0) + q_R(0)) + \sum_{k=1}^K \frac{P^{(k)}}{k!} \tau^k . \quad (53)$$

Remark: All coefficients involving $\alpha(q)$ and its derivatives are evaluated using the leading term $q(0, 0_+)$ of the expansion.

3.5 The Non-linear Inhomogeneous Case

Now we consider the full problem

$$\left. \begin{aligned} \partial_t q(x, t) &= \partial_x (\alpha(q(x, t)) \partial_x q(x, t)) + s(x, t, q(x, t)) , -\infty < x < \infty , t > 0 , \\ q(x, 0) &= \begin{cases} q_L(x) & \text{if } x < 0 , \\ q_R(x) & \text{if } x > 0 . \end{cases} \end{aligned} \right\} \quad (54)$$

Here the only difference to the previous simpler cases is given by the presence of the non-linear source term. For the time derivatives one obtains functions of space derivatives and derivatives of the source term with respect to the unknown $q(x, t)$. For example, for $k = 1$ we have

$$\partial_t q(x, t) = P^{(1)} = \alpha(q) \partial_x^{(2)} q(x, t) + \alpha'(q(x, t)) (\partial_x q(x, t))^2 + s(x, t, q(x, t)) . \quad (55)$$

As before, the calculation of higher order terms require the use of algebraic manipulators. Spatial derivatives are solutions to classical Riemann problems for spatial derivatives, as before. The final solution will have the same form as (53).

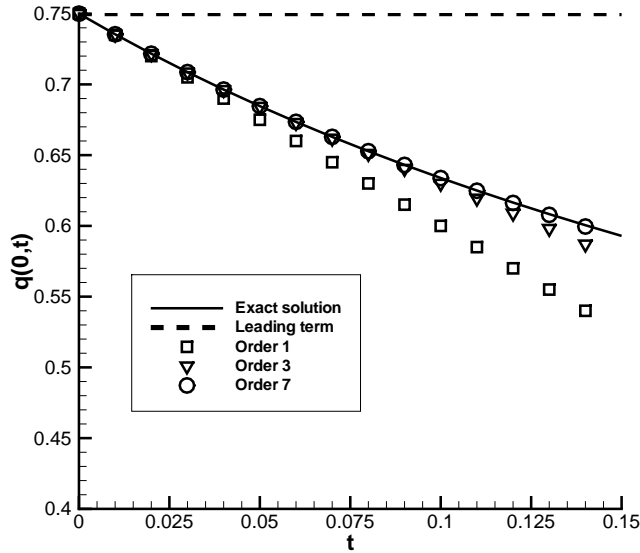


Figure 3: The Derivative Riemann Problem. Comparison of the approximate solution at $x = 0$ (symbols) with the exact solution (line) for the linear homogeneous case.

4 Assessment of the DRP Approximations

Here we assess the accuracy of the solution method for the Derivative Riemann Problem via some examples with exact solution.

4.1 The Linear Homogeneous Case

Let us consider the following Cauchy problem

$$\left. \begin{aligned} \partial_t q(x, t) &= \alpha \partial_x^{(2)} q(x, t), \quad -\infty < x < \infty, t > 0, \\ q(x, 0) &= \begin{cases} q_L(x) & \text{if } x < 0, \\ q_R(x) & \text{if } x > 0. \end{cases} \end{aligned} \right\} \quad (56)$$

The exact solution is

$$q(x, t) = \frac{1}{2\sqrt{\pi\alpha t}} \left[\int_{-\infty}^0 q_L(\xi) e^{-\frac{(x-\xi)^2}{4\alpha t}} d\xi + \int_0^{\infty} q_R(\xi) e^{-\frac{(x-\xi)^2}{4\alpha t}} d\xi \right], \quad (57)$$

which is used to assess the accuracy of the proposed approximate solutions. We consider the initial condition: $q_L(x) = e^{-x^2}$ and $q_R(x) = \frac{1}{2}e^{-x^2}$ and the diffusion coefficient $\hat{\alpha} = 1$.

Figure 3 shows the solution of the DRP at the position $x = 0$, as a function of time. Symbols represent the solution for different orders of the DRP approximate solution. It can be seen that when the order increases the accuracy increases. Table 1 shows the errors for different output times ($t = 0.01$, $t = 0.05$, $t = 0.1$, $t = 0.2$). When time increases there is a loss of accuracy, as the series expansion tends to loose validity.

<i>Order</i>	$t = 0.01$	$t = 0.05$	$t = 0.1$	$t = 0.2$
0	0.1456×10^{-1}	0.6535×10^{-1}	0.116×10^{-1}	0.1909×10^{-1}
1	0.4355×10^{-3}	0.9653×10^{-2}	0.3386×10^{-1}	0.1090×10^{-1}
2	0.1449×10^{-3}	0.1596×10^{-2}	0.1113×10^{-1}	0.7098×10^{-2}
3	0.5068×10^{-6}	0.2782×10^{-3}	0.3866×10^{-2}	0.4901×10^{-2}
4	0.1823×10^{-7}	0.4993×10^{-3}	0.1384×10^{-2}	0.3498×10^{-2}
5	0.6682×10^{-9}	0.9134×10^{-5}	0.5057×10^{-3}	0.2549×10^{-2}
6	0.2481×10^{-10}	0.1694×10^{-5}	0.1873×10^{-3}	0.1885×10^{-2}
7	0.9301×10^{-12}	0.3172×10^{-6}	0.7009×10^{-4}	0.1409×10^{-2}
8	0.3513×10^{-13}	0.5986×10^{-7}	0.2643×10^{-4}	0.1062×10^{-2}
9	0.1335×10^{-14}	0.1136×10^{-7}	0.1003×10^{-4}	0.8052×10^{-3}
10	0.5095×10^{-16}	0.2168×10^{-8}	0.3826×10^{-5}	0.6137×10^{-3}

Table 1: DRP solution errors for different output times and orders of accuracy. Linear homogeneous case.

<i>Order</i>	$t = 0.01$	$t = 0.05$	$t = 0.1$	$t = 0.2$
0	0.7173×10^{-2}	0.3024×10^{-1}	0.4947×10^{-1}	0.6722×10^{-1}
1	0.3267×10^{-3}	0.7256×10^{-2}	0.2553×10^{-1}	0.8278×10^{-1}
2	0.1074×10^{-4}	0.1181×10^{-2}	0.8220×10^{-2}	0.5221×10^{-1}
3	0.3814×10^{-6}	0.2092×10^{-3}	0.2905×10^{-2}	0.3678×10^{-1}
4	0.1382×10^{-7}	0.3783×10^{-4}	0.1048×10^{-2}	0.2647×10^{-1}
5	0.5089×10^{-9}	0.6955×10^{-5}	0.3849×10^{-3}	0.1939×10^{-1}
6	0.1896×10^{-10}	0.1294×10^{-5}	0.1431×10^{-3}	0.1439×10^{-1}
7	0.7126×10^{-12}	0.2429×10^{-6}	0.5367×10^{-4}	0.1079×10^{-1}
8	0.2696×10^{-13}	0.4594×10^{-7}	0.2028×10^{-4}	0.8145×10^{-2}
9	0.1026×10^{-14}	0.8734×10^{-8}	0.7709×10^{-5}	0.6186×10^{-2}
10	0.3922×10^{-16}	0.1668×10^{-8}	0.2944×10^{-5}	0.4722×10^{-2}

Table 2: DRP solution errors for different output times and orders of accuracy. Linear inhomogeneous case.

4.2 Linear Inhomogeneous Case

Now we consider the following Cauchy problem

$$\left. \begin{aligned} \partial_t q(x, t) &= \alpha \partial_x^{(2)} q(x, t) + \beta q(x, t), \quad -\infty < x < \infty, t > 0, \\ q(x, 0) &= \begin{cases} q_L(x) & \text{if } x < 0, \\ q_R(x) & \text{if } x > 0. \end{cases} \end{aligned} \right\} \quad (58)$$

where α and β are two constants. The approximate solution of the DRP is obtained as in (49) and is compared with the exact solution

$$q(x, t) = \frac{e^{\beta t}}{2\sqrt{\pi\alpha t}} \left[\int_{-\infty}^0 q_L(\xi) e^{-\frac{(x-\xi)^2}{4\alpha t}} d\xi + \int_0^{\infty} q_R(\xi) e^{-\frac{(x-\xi)^2}{4\alpha t}} d\xi \right]. \quad (59)$$

As initial condition we take $q_L(x) = e^{-x^2}$ and $q_R(x) = \frac{1}{2}e^{-x^2}$ with diffusion coefficient $\alpha = 1$ and reaction coefficient $\beta = 1$. Results are depicted in Figure 4, while the errors are shown in Table 2.

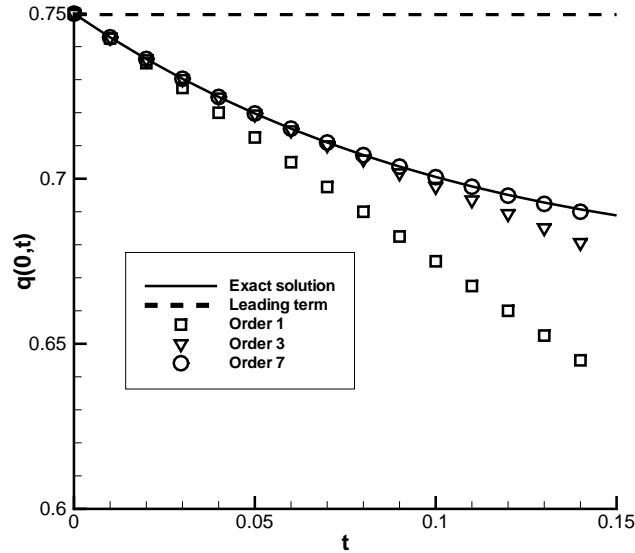


Figure 4: The Derivative Riemann Problem. Comparison of the approximate solution (symbols) with the exact solution (line) for the linear inhomogeneous case.

5 Reconstruction, Numerical Fluxes and Schemes

We now use local solutions of derivative Riemann problems to construct finite volume schemes of the form

$$q_i^{n+1} = q_i^n + \frac{\Delta t}{\Delta x} [g_{i+\frac{1}{2}} - g_{i-\frac{1}{2}}] + \Delta t s_i, \quad (60)$$

for which we need to specify the numerical flux $g_{i+1/2}$ and the numerical source s_i .

5.1 The High-Order Riemann Problem and Numerical Fluxes

The intercell flux at the interface position $x_{i+1/2}$ is defined as an approximation to the time integral average

$$g_{i+1/2} = -\frac{1}{\Delta t} \int_0^{\Delta t} \alpha(q(x_{i+1/2}, \tau)) \partial_x q(x_{i+1/2}, \tau) d\tau, \quad (61)$$

for which we need the functions of time $q(x_{i+1/2}, \tau)$ and $\partial_x q(x_{i+1/2}, \tau)$ at the interface, and which we denote respectively by $q_{LR}^{(0)}(\tau)$ and $q_{LR}^{(1)}(\tau)$.

5.1.1 Solution for the state variable

To find $q_{LR}^{(0)}(\tau)$ we solve the Derivative Riemann Problem

$$\left. \begin{aligned} \partial_t q(x, t) &= \partial_x (\alpha(q(x, t)) \partial_x q(x, t)) + s(x, t, q(x, t)), \quad -\infty < x < \infty, \quad t > 0, \\ q(x, 0) &= \begin{cases} p_i(x) & \text{if } x < 0, \\ p_{i+1}(x) & \text{if } x > 0, \end{cases} \end{aligned} \right\} \quad (62)$$

where $p_i(x)$ and $p_{i+1}(x)$ are polynomials to be obtained from a reconstruction procedure, to be detailed in the next subsection. The sought solution is expressed as the following power series

expansion

$$q_{LR}^{(0)}(\tau) = q(0, 0_+) + \sum_{k=1}^K \frac{\tau^k}{k!} \partial_t^{(k)} q(0, 0_+) + \mathcal{O}(\tau^{K+1}). \quad (63)$$

To find the leading term $q(0, 0_+)$ we linearize the equation in (62) and pose the linear, homogeneous conventional Riemann problem

$$\left. \begin{aligned} \partial_t q(x, t) &= \hat{\alpha} \partial_x^{(2)} q(x, t), \quad -\infty < x < \infty, t > 0, \\ q(x, 0) &= \begin{cases} p_i(0) & \text{if } x < 0, \\ p_{i+1}(0) & \text{if } x > 0, \end{cases} \end{aligned} \right\} \quad (64)$$

where $\hat{\alpha} = \alpha(\frac{1}{2}(p_i(0) + p_{i+1}(0)))$. The solution is

$$q(0, 0_+) = \frac{1}{2}(p_i(0) + p_{i+1}(0)). \quad (65)$$

To compute the higher order terms in (63) we use the Cauchy-Kowalewski procedure to express time derivatives as functions of space derivatives using fully the non-linear equation in (62), including the source term, namely

$$\partial_t^{(k)} q(0, 0_+) = P^{(k)} \left(\partial_x^{(0)} q(0, 0_+), \partial_x^{(2)} q(0, 0_+), \partial_x^{(4)} q(0, 0_+), \dots, \partial_x^{(2k)} q(0, 0_+) \right). \quad (66)$$

The space derivatives, which are the arguments of the functions $P^{(k)}$, are found by solving homogeneous, linearized classical Riemann problems for derivatives, see (44) to (46).

5.1.2 Solution for the gradient

To compute $q_{LR}^{(1)}(\tau)$ we assume an estimate $\partial_x q(0, 0_+)$ for the gradient at time $t = 0_+$. This estimate is calculated as in the process for obtaining the state variable q , see (44) to (46). Then we formally write a power series expansion for $q_{LR}^{(1)}(\tau) \equiv \partial_x q(0, t)$ about $t = 0_+$, at $x = 0$, namely

$$q_{LR}^{(1)}(\tau) = \partial_x q(0, 0_+) + \sum_{k=1}^K \frac{\tau^k}{k!} \partial_t^{(k)} (\partial_x q(0, 0_+)) + \mathcal{O}(\tau^{K+1}). \quad (67)$$

The leading term is already determined. The higher order terms are calculated by first transforming time derivatives to space derivatives, via Cauchy-Kowalewski procedure, namely

$$\partial_t^{(k)} (\partial_x q(0, 0_+)) = Q^{(k)} \left(\partial_x^{(0)} q(0, 0_+), \partial_x^{(1)} q(0, 0_+), \partial_x^{(3)} q(0, 0_+), \partial_x^{(5)} q(0, 0_+), \dots, \partial_x^{(2k+1)} q(0, 0_+) \right). \quad (68)$$

We note that to obtain the function $Q^{(k)}$ we use the full non-linear equation, including the source term, if present. The spatial derivatives, which are the arguments of $Q^{(k)}$, are obtained as for the solution of the state variable at the interface, namely, we solve linearized Riemann problems for spatial derivatives, see (44) to (46).

5.1.3 Reconstruction

In order to solve the derivative Riemann problem (62) we need to provide the initial conditions knowing only the set of cell averages $\{q_i^n\}$. To accomplish this we perform a reconstruction procedure, as done for modern shock-capturing methods for hyperbolic balance laws, generating in this manner piece-wise polynomial functions $p_i(x)$ for each cell I_i . If we wish to get an order

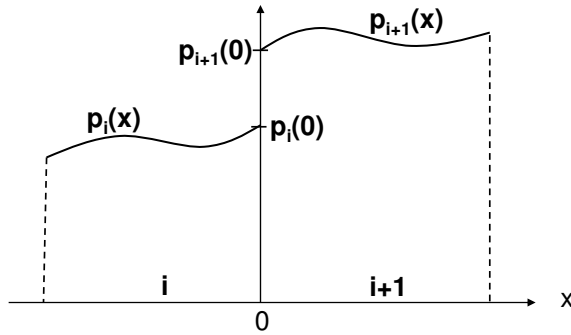


Figure 5: Initial condition for the Derivative Riemann Problem used in the reconstruction process.

$\mathcal{O}(\tau^{K+1})$ in expansions (63) and (67), the polynomial $p_i(x)$ must have degree, at least, $2K + 1$, in order to be able to evaluate all the derivatives in (66), (68). This polynomial can be expressed as

$$p_i(x) = \sum_{k=0}^{2K+1} c_k x^k, \quad (69)$$

where the coefficients c_k , ($k = 0, 1, \dots, 2K + 1$) are to be determined from $2(K + 1)$ conditions that may be obtained from *conservation requirements*. To enforce conservation several techniques can be applied [12, 20]. Let us assume that the polynomial $p_i(x)$ passes through $2K + 2$ cells

$$\{i - s_0, i - s_0 + 1, \dots, i - s_0 + 2K + 1\},$$

where the value of s_0 will be discussed later. We choose to apply reconstructions that are conservative and to some extent non-linear, as we shall explain below. Conservation requires

$$q_j^n = \frac{1}{\Delta x} \int_{x_{j-1/2}}^{x_{j+1/2}} p_i(\xi) d\xi, \quad (j = i - s_0, i - s_0 + 1, \dots, i - s_0 + 2K + 1), \quad (70)$$

where q_j^n is the spatial average of the function $q(x, t^n)$ in the cell $I_j = [x_{j-1/2}, x_{j+1/2}]$. Conditions (70) result in a system of algebraic equations for the coefficients $\{c_k\}_{k=0}^{2K+1}$ in (69). Having obtained the polynomial $p_i(x)$ the spatial derivatives needed are given by

$$\partial_x^{(k)} q(0, 0_+) = \frac{d^k}{dx^k} p_i(0). \quad (71)$$

In this manner the local initial conditions for the Derivative Riemann Problem (62) are determined as $q_L(x) \equiv p_i(x)$, $q_R(x) \equiv p_{i+1}(x)$. Figure 5 depicts the form of the initial conditions. Using the solution procedure studied in Section 4 we can determine (63) and (67) and thus (61) can be evaluated.

5.1.4 Choice of the stencil

We have developed the schemes ADER-DR $_{n,m}$ (**ADER** for **D**iffusion **R**eaction) where the subscript $n = 3, 4, \dots, 10$ indicates the degree of the interpolation polynomial used, while the subscript $m = 2, 3, \dots, 5$ denotes the degree of the time series expansion in the solution of the DRP.

We have implemented non-linear ENO reconstruction schemes with a restricted range in the choice of the stencil. The restriction favours centred stencils, excluding fully one-sided and

<i>Scheme</i>	s_0
<i>ADER</i> – <i>DR</i> _{3,2}	2, 1
<i>ADER</i> – <i>DR</i> _{4,2}	3, 2, 1
<i>ADER</i> – <i>DR</i> _{5,3}	3, 2
<i>ADER</i> – <i>DR</i> _{6,3}	4, 3, 2
<i>ADER</i> – <i>DR</i> _{7,4}	4, 3, 2
<i>ADER</i> – <i>DR</i> _{8,4}	5, 4, 3
<i>ADER</i> – <i>DR</i> _{9,5}	6, 5, 4, 3
<i>ADER</i> – <i>DR</i> _{10,5}	7, 6, 5, 4, 3

Table 3: Choice of the index s_0 for each one of the ADER schemes for diffusion.

highly biased stencils. The rationale behind is that centred stencils are the best choice from the point of view of accuracy and stability, even for hyperbolic problems [34], for which non-linear reconstructions are mandatory in order to circumvent Godunov’s theorem. For diffusion-reaction equations we have performed extensive numerical experiments, arriving at similar conclusions. As a matter of fact, for most situations one can use a *linear reconstruction* with a fixed stencil, a centred or quasi-centred stencil. The results reported here are all based on the restricted ENO reconstruction, for which the choice of admissible values of the index s_0 in (70) has been based on numerical experiments. Results are shown in the Table 3. For instance, the scheme *ADER* – *DR*_{4,2} uses the stencils $\{i - 3, i - 2, i - 1, i, i + 1\}$, $\{i - 2, i - 1, i, i + 1, i + 2\}$ and $\{i - 1, i, i + 1, i + 2, i + 3\}$.

5.2 Numerical source

To determine the numerical source s_i in the finite volume scheme (4) we compute the space-time average

$$s_i = \frac{1}{\Delta x} \int_{x_{i-1/2}}^{x_{i+1/2}} \frac{1}{\Delta t} \left[\int_0^{\Delta t} s(x, \tau, q(x, \tau)) d\tau \right] dx \quad (72)$$

using a numerical quadrature formula. To get good accuracy in the space and time integration, we can use a Gaussian quadrature rule, with N points in space and N points in time, so that we can write

$$s_i = \frac{1}{\Delta x} \sum_{j=1}^N \left\{ \omega_j \left(\frac{1}{\Delta t} \sum_{l=1}^N \delta_l s(x_l, \tau_l, q(x_j, \tau_l)) \right) \right\}, \quad (73)$$

where (δ_l, τ_l) are the weights and points used in time integration, while (ω_j, x_j) are the weights and points used in space integration. The function values $q(x_j, \tau_l)$ are obtained from the Cauchy-Kowalewski method.

5.3 Example

Let us consider the Cauchy diffusion-reaction problem

$$\left. \begin{aligned} \partial_t q(x, t) &= \hat{\alpha} \partial_x^{(2)} q(x, t) + \beta q(x, t), \\ q(x, 0) &= q^{(0)}(x), \end{aligned} \right\} \quad (74)$$

where α and β are constants. If we take the scheme *ADER-DR*_{3,2} with $s_0 = 2$, which means that we are choosing the fixed stencil $\{i - 2, i - 1, i, i + 1\}$, and apply the procedure described

in sections 5.1 and 5.2, we obtain the final expression for the scheme as

$$q_i^{n+1} = \sum_{l=-3}^2 b_l q_{i+l}^n, \quad (75)$$

with

$$\left. \begin{aligned} b_{-3} &= -\frac{1}{24}d(1-6d) - \frac{1}{48}rd, \\ b_{-2} &= \frac{1}{24}d(3-18d) + \frac{1}{16}rd, \\ b_{-1} &= \frac{1}{24}d(22+12d) + \frac{11}{24}rd + \frac{1}{2}rd, \\ b_0 &= 1 - \frac{1}{24}d(50-12d) - \frac{25}{24}rd + r(1-d + \frac{1}{2}r), \\ b_1 &= \frac{1}{24}d(27-18d) + \frac{9}{16}rd + \frac{1}{2}rd, \\ b_2 &= -\frac{1}{24}d(1-6d) - \frac{1}{48}rd \end{aligned} \right\} \quad (76)$$

and $d = \frac{\hat{\alpha}\Delta t}{\Delta x^2}$ and $r = \Delta t\beta$.

6 Convergence Rates Study

In this section we perform a detailed study of the convergence rates for the high-order schemes developed, in order to verify that the expected orders of accuracy hold in practice.

6.1 Empirical order of accuracy

The procedure to obtain empirically the order of accuracy of a scheme consists of considering a set of M regular meshes of sizes $\{\Delta x_k\}_{k=1}^M$. These meshes are then used to obtain numerical solutions and corresponding errors $\{\|\epsilon_k\|\}_{k=1}^M$, assuming the exact or a reference solution is known. The error satisfies

$$\|\epsilon_k\| \leq C(\Delta x_k)^p, \quad (77)$$

where C is a constant independent of the mesh and p is the order of accuracy of the scheme, to be determined. For our study we use the sequence of meshes $\Delta x_k = \frac{\Delta x_{k-1}}{2}$, ($k = 2, 3, \dots, M$) and apply the following sequence of steps

1. Computation of the numerical solution with the first mesh.
2. Computation of the error $\|\epsilon_1\|$ on a chosen norm.
3. For $k=2, M$ do
 - (a) Computation of the numerical solution with mesh k .
 - (b) Evaluation of the error $\|\epsilon_k\|$.
 - (c) Calculation of the order $p = \frac{\log \frac{\|\epsilon_{k-1}\|}{\|\epsilon_k\|}}{\log 2}$.
4. End of k

The process just described will give the sought value of p , which is the order of accuracy of the scheme.

The following subsections are devoted to analyze the accuracy of the schemes described in Section 5 applied to four test cases. To perform this study we obtain numerical solutions for four different meshes of 20, 40, 80, 160 cells, for the linear case, and 15, 30, 60, 120 for the nonlinear case. Results of up to 10^{th} order of accuracy have been obtained. To measure the error we have used the norms L_1 , L_2 and L_∞ .

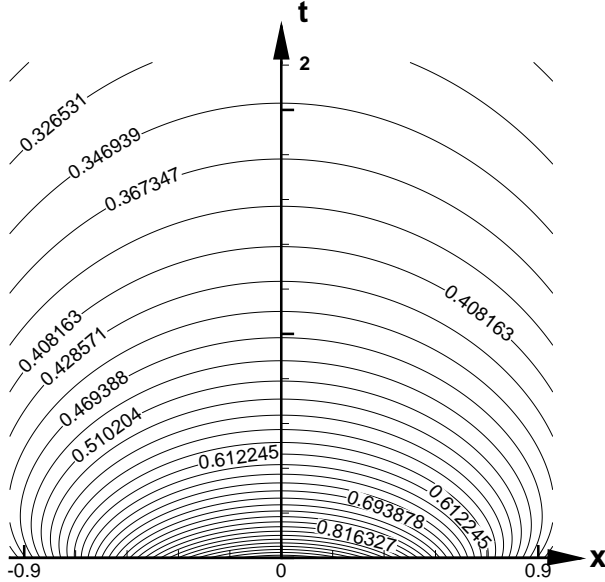


Figure 6: Contour plot $x - t$ of solution for linear homogeneous problem.

As can be seen in (66)-(68), to have an order $\mathcal{O}(\tau^{K+1})$ in the DRP solution, we need a reconstruction polynomial of degree at least $2K + 1$; this means that to obtain $\mathcal{O}(\tau^2)$ we need at least a third degree polynomial but, to get one more order, $\mathcal{O}(\tau^3)$, we need a fifth degree polynomial, and so on. We shall see in the examples below that the empirical order of accuracy is close to the degree of the polynomial used in the reconstruction.

In all the examples described the chosen output time is $t = 0.5$ and the diffusion coefficient to calculate the time step is $d = 0.5$. The time step, at any time level n , is calculated according to the formula $\Delta t = \frac{d\Delta x^2}{\alpha_{max}}$, where α_{max} is the largest value of the diffusion coefficient in the domain, at the time level considered.

6.2 The Linear Homogeneous Case

As a first example we consider the linear diffusion problem

$$\left. \begin{aligned} \partial_t q(x, t) &= \partial_x^{(2)} q(x, t), \quad -10 < x < 10, t > 0, \\ q(x, 0) &= e^{-x^2}. \end{aligned} \right\} \quad (78)$$

The exact solution to this problem is

$$q(x, t) = \frac{1}{2\sqrt{\pi t}} \int_{-10}^{10} e^{-\left[\xi^2 + \frac{(x-\xi)^2}{4\alpha t}\right]} d\xi. \quad (79)$$

Figure 6 depicts the contour plot of the analytical solution in time and space. Convergence rates results for this test problem are shown in Table 4. We use four meshes ($M = 4$), with 20, 40, 80 and 160 cells respectively. We calculate the errors with the norms L_1 , L_2 and L_∞ and obtain the corresponding orders p_1 , p_2 and p_∞ from the procedure described above. Results have been obtained for the schemes ADER-DR $_{n,m}$ ($n = 3, \dots, 10$; $m = 2, \dots, 5$), described in Section 5.

<i>Cells</i>	L_1	p_1	L_2	p_2	L_∞	p_∞
ADER-DR_{3,2}						
20	0.20×10^{-1}		0.42×10^{-1}		0.94×10^{-1}	
40	0.15×10^{-2}	3.75	0.28×10^{-2}	3.89	0.90×10^{-2}	3.39
80	0.14×10^{-3}	3.36	0.29×10^{-3}	3.28	0.12×10^{-2}	2.94
160	0.16×10^{-4}	3.16	0.33×10^{-4}	3.16	0.14×10^{-3}	3.08
ADER-DR_{4,2}						
20	0.12×10^{-1}		0.25×10^{-1}		0.57×10^{-1}	
40	0.69×10^{-3}	4.16	0.13×10^{-2}	4.29	0.33×10^{-2}	4.10
80	0.49×10^{-4}	3.81	0.87×10^{-4}	3.86	0.23×10^{-3}	3.82
160	0.55×10^{-5}	3.18	0.99×10^{-5}	3.14	0.24×10^{-4}	3.28
ADER-DR_{5,3}						
20	0.44×10^{-2}		0.89×10^{-2}		0.22×10^{-1}	
40	0.11×10^{-3}	5.34	0.25×10^{-3}	5.15	0.90×10^{-3}	4.58
80	0.29×10^{-5}	5.21	0.62×10^{-5}	5.34	0.24×10^{-4}	5.22
160	0.88×10^{-7}	5.05	0.18×10^{-6}	5.08	0.73×10^{-6}	5.05
ADER-DR_{6,3}						
20	0.39×10^{-2}		0.80×10^{-2}		0.19×10^{-1}	
40	0.60×10^{-4}	6.05	0.12×10^{-3}	6.06	0.32×10^{-3}	5.92
80	0.82×10^{-6}	6.19	0.15×10^{-5}	6.28	0.40×10^{-5}	6.31
160	0.14×10^{-7}	5.92	0.25×10^{-7}	5.93	0.67×10^{-7}	5.91
ADER-DR_{7,4}						
20	0.27×10^{-2}		0.72×10^{-2}		0.24×10^{-1}	
40	0.25×10^{-4}	6.76	0.57×10^{-4}	6.96	0.25×10^{-3}	6.57
80	0.11×10^{-6}	7.75	0.25×10^{-6}	7.86	0.12×10^{-5}	7.69
160	0.61×10^{-9}	7.55	0.13×10^{-8}	7.57	0.66×10^{-8}	7.54
ADER-DR_{8,4}						
20	0.52×10^{-3}		0.10×10^{-2}		0.25×10^{-2}	
40	0.22×10^{-5}	7.87	0.44×10^{-5}	7.82	0.14×10^{-4}	7.45
80	0.13×10^{-7}	7.43	0.26×10^{-7}	7.39	0.84×10^{-7}	7.40
160	0.58×10^{-10}	7.78	0.12×10^{-9}	7.80	0.37×10^{-9}	7.81
ADER-DR_{9,5}						
20	0.67×10^{-3}		0.13×10^{-2}		0.33×10^{-2}	
40	0.16×10^{-5}	8.68	0.35×10^{-5}	8.57	0.14×10^{-4}	7.88
80	0.42×10^{-8}	8.61	0.85×10^{-8}	8.68	0.29×10^{-7}	8.93
160	0.79×10^{-11}	9.04	0.16×10^{-10}	9.07	0.56×10^{-10}	9.01
ADER-DR_{10,5}						
20	0.85×10^{-3}		0.17×10^{-2}		0.42×10^{-2}	
40	0.16×10^{-5}	9.03	0.36×10^{-5}	8.92	0.13×10^{-4}	8.31
80	0.91×10^{-9}	10.80	0.18×10^{-8}	10.93	0.68×10^{-8}	10.92
160	0.59×10^{-12}	10.61	0.12×10^{-11}	10.61	0.42×10^{-11}	10.68

Table 4: Convergence rates for the linear homogeneous example.

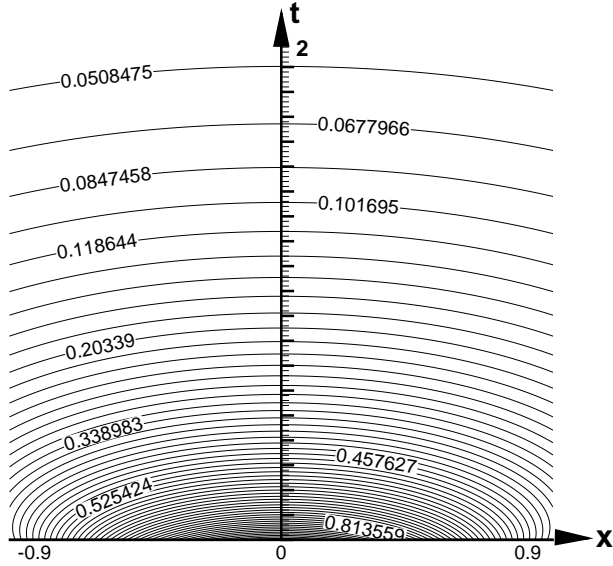


Figure 7: Contour plot $x - t$ of solution for linear inhomogeneous problem.

6.3 The Linear Inhomogeneous Case

We consider the linear diffusion problem with a reaction term

$$\left. \begin{aligned} \partial_t q(x, t) &= \partial_x^{(2)} q(x, t) - q(x, t), \quad -10 < x < 10, t > 0, \\ q(x, 0) &= e^{-x^2}. \end{aligned} \right\} \quad (80)$$

The exact solution is

$$q(x, t) = e^t \left[\frac{1}{2\sqrt{\pi t}} \int_{-10}^{10} e^{-\left[\xi^2 + \frac{(x-\xi)^2}{4\alpha t}\right]} d\xi \right]. \quad (81)$$

Figure 7 depicts the contour plot in space and time of the exact solution, given by (81). In Table 5 we show the empirical orders of accuracy obtained when using the ADER-DR $_{n,m}$ schemes described in Section 5.

6.4 The Non-linear Homogeneous Case

Now we consider the problem

$$\left. \begin{aligned} \partial_t q(x, t) &= \partial_x \left((q(x, t))^{-1} \partial_x q(x, t) \right), \quad -4.5 < x < 4.5, t > 0, \\ q(x, 0) &= \frac{\sinh(2)}{\cosh(2) - \sin(\sqrt{2}(x-1))}. \end{aligned} \right\} \quad (82)$$

The exact solution [31] is

$$q(x, t) = \frac{\sinh(2t + 2)}{\cosh(2t + 2) - \sin(\sqrt{2}(x - 1))}. \quad (83)$$

This solution is periodic with period $\frac{\sqrt{2}}{\pi}$. Figure 8 depicts the corresponding contour plot. Table 6 shows the empirical orders of accuracy obtained when using the schemes described in Section 5.

<i>Cells</i>	L_1	p_1	L_2	p_2	L_∞	p_∞
ADER-DR_{3,2}						
20	0.12×10^{-1}		0.29×10^{-1}		0.10×10^0	
40	0.78×10^{-3}	4.00	0.16×10^{-2}	4.12	0.65×10^{-2}	3.97
80	0.80×10^{-4}	3.28	0.16×10^{-3}	3.35	0.58×10^{-3}	3.48
160	0.95×10^{-5}	3.07	0.19×10^{-4}	3.09	0.65×10^{-4}	3.15
ADER-DR_{4,2}						
20	0.57×10^{-2}		0.12×10^{-1}		0.34×10^{-1}	
40	0.31×10^{-3}	4.19	0.61×10^{-3}	4.29	0.17×10^{-2}	4.33
80	0.21×10^{-4}	3.89	0.39×10^{-4}	3.94	0.11×10^{-3}	3.90
160	0.22×10^{-5}	3.27	0.40×10^{-5}	3.28	0.11×10^{-4}	3.35
ADER-DR_{5,3}						
20	0.24×10^{-2}		0.45×10^{-2}		0.11×10^{-1}	
40	0.35×10^{-4}	6.12	0.84×10^{-4}	5.73	0.31×10^{-3}	5.14
80	0.12×10^{-5}	4.84	0.26×10^{-5}	5.04	0.10×10^{-4}	4.96
160	0.44×10^{-7}	4.80	0.90×10^{-7}	4.82	0.36×10^{-6}	4.78
ADER-DR_{6,3}						
20	0.35×10^{-2}		0.65×10^{-2}		0.16×10^{-1}	
40	0.39×10^{-4}	6.50	0.82×10^{-4}	6.31	0.27×10^{-3}	5.92
80	0.63×10^{-6}	5.93	0.13×10^{-5}	6.02	0.46×10^{-5}	5.86
160	0.10×10^{-7}	5.92	0.20×10^{-7}	5.98	0.67×10^{-7}	6.10
ADER-DR_{7,4}						
20	0.32×10^{-2}		0.63×10^{-2}		0.19×10^{-1}	
40	0.17×10^{-4}	7.57	0.38×10^{-4}	7.36	0.15×10^{-3}	6.98
80	0.73×10^{-7}	7.84	0.16×10^{-6}	7.92	0.73×10^{-6}	7.71
160	0.38×10^{-9}	7.59	0.80×10^{-9}	7.64	0.39×10^{-8}	7.53
ADER-DR_{8,4}						
20	0.23×10^{-2}		0.40×10^{-2}		0.78×10^{-2}	
40	0.73×10^{-5}	8.32	0.17×10^{-4}	7.87	0.66×10^{-4}	6.88
80	0.26×10^{-7}	8.14	0.53×10^{-7}	8.34	0.21×10^{-6}	8.29
160	0.10×10^{-9}	8.00	0.20×10^{-9}	8.04	0.75×10^{-9}	8.14
ADER-DR_{9,5}						
20	0.38×10^{-3}		0.86×10^{-3}		0.26×10^{-2}	
40	0.10×10^{-5}	8.50	0.22×10^{-5}	8.63	0.73×10^{-5}	8.50
80	0.28×10^{-8}	8.51	0.60×10^{-8}	8.51	0.21×10^{-7}	8.47
160	0.53×10^{-11}	9.06	0.11×10^{-10}	9.09	0.35×10^{-10}	9.20
ADER-DR_{10,5}						
20	0.80×10^{-3}		0.20×10^{-2}		0.62×10^{-2}	
40	0.18×10^{-5}	8.79	0.45×10^{-5}	8.78	0.19×10^{-4}	8.36
80	0.13×10^{-8}	10.43	0.28×10^{-8}	10.66	0.12×10^{-7}	10.64
160	0.12×10^{-11}	10.10	0.24×10^{-11}	10.20	0.96×10^{-11}	10.28

Table 5: Convergence rates for the linear inhomogeneous example.

<i>Cells</i>	L_1	p_1	L_2	p_2	L_∞	p_∞
ADER-DR_{3,2}						
15	0.25×10^{-2}		0.29×10^{-2}		0.57×10^{-2}	
30	0.29×10^{-3}	3.10	0.35×10^{-3}	3.03	0.66×10^{-3}	3.11
60	0.33×10^{-4}	3.12	0.43×10^{-4}	3.06	0.79×10^{-4}	3.06
120	0.40×10^{-5}	3.05	0.53×10^{-5}	3.02	0.96×10^{-5}	3.05
ADER-DR_{4,2}						
15	0.11×10^{-2}		0.13×10^{-2}		0.29×10^{-2}	
30	0.59×10^{-4}	4.27	0.71×10^{-4}	4.24	0.15×10^{-3}	4.27
60	0.49×10^{-5}	3.59	0.56×10^{-5}	3.68	0.10×10^{-4}	3.87
120	0.58×10^{-6}	3.09	0.64×10^{-6}	3.14	0.93×10^{-6}	3.45
ADER-DR_{5,3}						
15	0.32×10^{-3}		0.37×10^{-3}		0.60×10^{-3}	
30	0.86×10^{-5}	5.22	0.10×10^{-4}	5.17	0.21×10^{-4}	4.86
60	0.23×10^{-6}	5.22	0.29×10^{-6}	5.14	0.69×10^{-6}	4.90
120	0.64×10^{-8}	5.16	0.79×10^{-8}	5.18	0.19×10^{-7}	5.15
ADER-DR_{6,3}						
15	0.33×10^{-3}		0.39×10^{-3}		0.63×10^{-3}	
30	0.52×10^{-5}	5.96	0.64×10^{-5}	5.91	0.14×10^{-4}	5.51
60	0.75×10^{-7}	6.13	0.95×10^{-7}	6.08	0.23×10^{-6}	5.89
120	0.11×10^{-8}	6.14	0.14×10^{-8}	6.13	0.34×10^{-8}	6.09
ADER-DR_{7,4}						
15	0.20×10^{-3}		0.25×10^{-3}		0.54×10^{-3}	
30	0.62×10^{-6}	8.31	0.68×10^{-6}	8.54	0.11×10^{-5}	8.99
60	0.66×10^{-8}	6.55	0.77×10^{-8}	6.47	0.15×10^{-7}	6.14
120	0.60×10^{-10}	6.79	0.69×10^{-10}	6.79	0.14×10^{-9}	6.77
ADER-DR_{8,4}						
15	0.14×10^{-3}		0.17×10^{-3}		0.31×10^{-3}	
30	0.35×10^{-6}	8.65	0.43×10^{-6}	8.62	0.85×10^{-6}	8.50
60	0.14×10^{-8}	7.94	0.19×10^{-8}	7.80	0.47×10^{-8}	7.48
120	0.52×10^{-11}	8.09	0.71×10^{-11}	8.09	0.18×10^{-10}	8.07
ADER-DR_{9,5}						
15	0.84×10^{-4}		0.92×10^{-4}		0.15×10^{-3}	
30	0.24×10^{-7}	11.76	0.31×10^{-7}	11.53	0.66×10^{-7}	11.11
60	0.65×10^{-10}	8.55	0.77×10^{-10}	8.66	0.17×10^{-9}	8.59
120	0.12×10^{-12}	9.06	0.14×10^{-12}	9.07	0.30×10^{-12}	9.18
ADER-DR_{10,5}						
15	0.79×10^{-4}		0.91×10^{-4}		0.17×10^{-3}	
30	0.31×10^{-7}	11.30	0.40×10^{-7}	11.17	0.83×10^{-7}	11.02
60	0.45×10^{-10}	9.46	0.63×10^{-10}	9.28	0.18×10^{-9}	8.83
120	0.46×10^{-13}	9.92	0.63×10^{-13}	9.98	0.18×10^{-12}	9.97

Table 6: Convergence rates for the nonlinear homogeneous example.

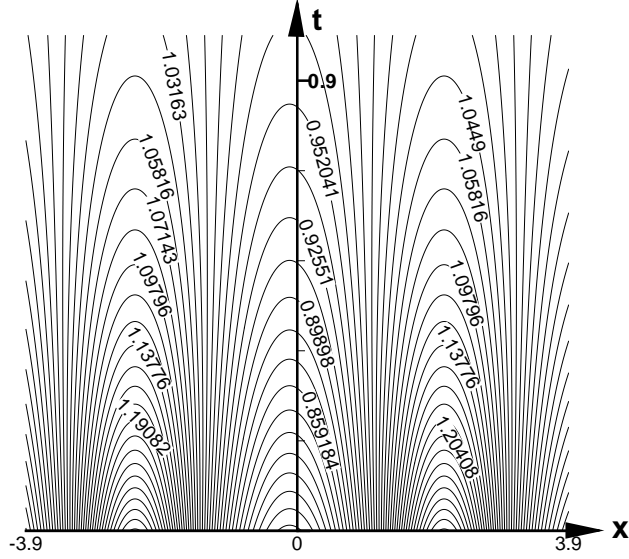


Figure 8: Contour plot $x - t$ of solution for nonlinear inhomogeneous problem.

6.5 The Non-linear Inhomogeneous Case

The last test case consists of a nonlinear diffusion equation with source term

$$\left. \begin{aligned} \partial_t q(x, t) &= \partial_x \left((q(x, t))^{-1} \partial_x q(x, t) \right) + s(x, t, q(x, t)), \quad -\infty < x < \infty, t > 0, \\ q(x, 0) &= \sinh(2) [\cosh(2) - \sin(\sqrt{2}(x-1))]^{-1}, \end{aligned} \right\} \quad (84)$$

where the source has the expression

$$s(x, t, q(x, t)) = q(x, t) + \frac{\sinh(2t+2) (\sin(\sqrt{2}(x-1)) - \cosh(2t+2))}{(\cosh(2t+2) - \sin(\sqrt{2}(x-1)))^2}. \quad (85)$$

Table 7 shows the empirical orders of accuracy obtained when using the schemes described in Section 5.

The convergence rates study just performed gives the empirical orders of accuracy and these are in agreement with the theoretically expected orders of accuracy for the schemes developed in this paper.

7 Numerical Examples

To illustrate the practical applicability of the methods we show numerical results for two examples. The first one is

$$\left. \begin{aligned} \partial_t q(x, t) &= \rho \partial_x [q(x, t) (1 - q(x, t)) \partial_x q(x, t)], \quad x \in \left[-\frac{1}{2}, \frac{1}{2}\right], \\ q(x, 0) &= \begin{cases} 1 & \text{if } x < 0, \\ 0 & \text{if } x > 0, \end{cases} \end{aligned} \right\} \quad (86)$$

with $0 \leq \rho < 1$. The equation arises in plasma physics, where the unknown $q(x, t)$ is the mass fraction of one component of the plasma. One remarkable aspect of this parabolic equation with

<i>Cells</i>	L_1	p_1	L_2	p_2	L_∞	p_∞
ADER-DR_{3,2}						
15	0.28×10^{-2}		0.32×10^{-2}		0.62×10^{-2}	
30	0.35×10^{-3}	3.01	0.43×10^{-3}	2.93	0.77×10^{-3}	3.02
60	0.41×10^{-4}	3.09	0.52×10^{-4}	3.03	0.95×10^{-4}	3.01
120	0.50×10^{-5}	3.04	0.65×10^{-5}	3.01	0.12×10^{-4}	3.04
ADER-DR_{4,2}						
15	0.14×10^{-2}		0.17×10^{-2}		0.36×10^{-2}	
30	0.11×10^{-3}	3.69	0.13×10^{-3}	3.77	0.25×10^{-3}	3.84
60	0.87×10^{-5}	3.64	0.99×10^{-5}	3.69	0.17×10^{-4}	3.85
120	0.89×10^{-6}	3.30	0.99×10^{-6}	3.33	0.14×10^{-5}	3.62
ADER-DR_{5,3}						
15	0.23×10^{-3}		0.27×10^{-3}		0.57×10^{-3}	
30	0.86×10^{-5}	4.71	0.10×10^{-4}	4.74	0.19×10^{-4}	4.88
60	0.27×10^{-6}	5.03	0.33×10^{-6}	4.93	0.78×10^{-6}	4.64
120	0.78×10^{-8}	5.08	0.97×10^{-8}	5.11	0.23×10^{-7}	5.08
ADER-DR_{6,3}						
15	0.27×10^{-3}		0.31×10^{-3}		0.57×10^{-3}	
30	0.57×10^{-5}	5.56	0.72×10^{-5}	5.45	0.16×10^{-4}	5.15
60	0.88×10^{-7}	6.01	0.12×10^{-6}	5.93	0.30×10^{-6}	5.77
120	0.13×10^{-8}	6.09	0.17×10^{-8}	6.08	0.44×10^{-8}	6.06
ADER-DR_{7,4}						
15	0.25×10^{-3}		0.32×10^{-3}		0.66×10^{-3}	
30	0.85×10^{-6}	8.17	0.92×10^{-6}	8.43	0.14×10^{-5}	8.86
60	0.87×10^{-8}	6.62	0.98×10^{-8}	6.55	0.19×10^{-7}	6.22
120	0.79×10^{-10}	6.78	0.91×10^{-10}	6.75	0.18×10^{-9}	6.75
ADER-DR_{8,4}						
15	0.18×10^{-3}		0.22×10^{-3}		0.41×10^{-3}	
30	0.33×10^{-6}	9.09	0.40×10^{-6}	9.11	0.86×10^{-6}	8.90
60	0.15×10^{-8}	7.85	0.21×10^{-8}	7.60	0.54×10^{-8}	7.30
120	0.56×10^{-11}	8.03	0.77×10^{-11}	8.06	0.21×10^{-10}	8.03
ADER-DR_{9,5}						
15	0.98×10^{-4}		0.11×10^{-3}		0.19×10^{-3}	
30	0.50×10^{-7}	10.94	0.66×10^{-7}	10.68	0.13×10^{-6}	10.54
60	0.72×10^{-10}	9.44	0.88×10^{-10}	9.54	0.17×10^{-9}	9.52
120	0.14×10^{-12}	8.99	0.16×10^{-12}	9.08	0.27×10^{-12}	9.33
ADER-DR_{10,5}						
15	0.82×10^{-4}		0.94×10^{-4}		0.18×10^{-3}	
30	0.36×10^{-7}	11.15	0.49×10^{-7}	10.90	0.12×10^{-6}	10.60
60	0.55×10^{-10}	9.34	0.69×10^{-10}	9.48	0.16×10^{-9}	9.50
120	0.57×10^{-13}	9.92	0.73×10^{-13}	9.89	0.20×10^{-12}	9.67

Table 7: Convergence rates for the nonlinear inhomogeneous example.

<i>Cells</i>	L_1	p_1	L_2	p_2	L_∞	p_∞
ADER-DR_{3,2}						
20	0.11×10^{-1}		0.25×10^{-1}		0.70×10^{-1}	
40	0.13×10^{-2}	3.00	0.36×10^{-2}	2.79	0.12×10^{-1}	2.61
80	0.16×10^{-3}	3.10	0.48×10^{-3}	2.91	0.25×10^{-2}	2.21
160	0.15×10^{-4}	3.41	0.49×10^{-4}	3.30	0.32×10^{-3}	2.96
ADER-DR_{4,2}						
20	0.10×10^{-1}		0.24×10^{-1}		0.68×10^{-1}	
40	0.72×10^{-3}	3.79	0.20×10^{-2}	3.54	0.73×10^{-2}	3.21
80	0.32×10^{-4}	4.49	0.10×10^{-3}	4.31	0.46×10^{-3}	4.00
160	0.21×10^{-5}	3.92	0.60×10^{-5}	4.11	0.27×10^{-4}	4.06
ADER-DR_{5,3}						
20	0.15×10^{-1}		0.34×10^{-1}		0.87×10^{-1}	
40	0.21×10^{-3}	6.16	0.74×10^{-3}	5.52	0.32×10^{-2}	4.74
80	0.78×10^{-5}	4.77	0.27×10^{-4}	4.80	0.13×10^{-3}	4.60
160	0.15×10^{-6}	5.65	0.55×10^{-6}	5.60	0.39×10^{-5}	5.09
ADER-DR_{6,3}						
20	0.14×10^{-1}		0.32×10^{-1}		0.82×10^{-1}	
40	0.32×10^{-3}	5.47	0.97×10^{-3}	5.06	0.41×10^{-2}	4.32
80	0.37×10^{-5}	6.44	0.12×10^{-4}	6.35	0.53×10^{-4}	6.25
160	0.52×10^{-7}	6.15	0.16×10^{-6}	6.18	0.98×10^{-6}	5.77
ADER-DR_{7,4}						
20	0.17×10^0		0.38×10^0		0.10×10^1	
40	0.17×10^{-2}	6.59	0.64×10^{-2}	5.91	0.36×10^{-1}	4.85
80	0.11×10^{-5}	10.67	0.31×10^{-5}	10.98	0.13×10^{-4}	11.45
160	0.38×10^{-8}	8.14	0.12×10^{-7}	8.05	0.70×10^{-7}	7.52
ADER-DR_{8,4}						
20	0.18×10^0		0.40×10^0		0.91×10^0	
40	0.53×10^{-3}	8.42	0.16×10^{-2}	7.94	0.72×10^{-2}	6.98
80	0.64×10^{-6}	9.69	0.19×10^{-5}	9.76	0.75×10^{-5}	9.90
160	0.12×10^{-8}	9.04	0.41×10^{-8}	8.85	0.26×10^{-7}	8.18
ADER-DR_{9,5}						
20	0.77×10^0		0.17×10^1		0.39×10^1	
40	0.53×10^{-2}	7.18	0.15×10^{-1}	6.87	0.53×10^{-1}	6.20
80	0.16×10^{-6}	15.05	0.59×10^{-6}	14.62	0.34×10^{-5}	13.92
160	0.12×10^{-9}	10.39	0.39×10^{-9}	10.56	0.23×10^{-8}	10.53
ADER-DR_{10,5}						
20	0.56×10^0		0.12×10^1		0.28×10^1	
40	0.13×10^{-1}	5.42	0.38×10^{-1}	5.01	0.13×10^0	4.39
80	0.12×10^{-6}	16.72	0.38×10^{-6}	16.61	0.21×10^{-5}	15.92
160	0.37×10^{-10}	11.66	0.13×10^{-9}	11.57	0.82×10^{-9}	11.36

Table 8: Convergence rates for example (88).

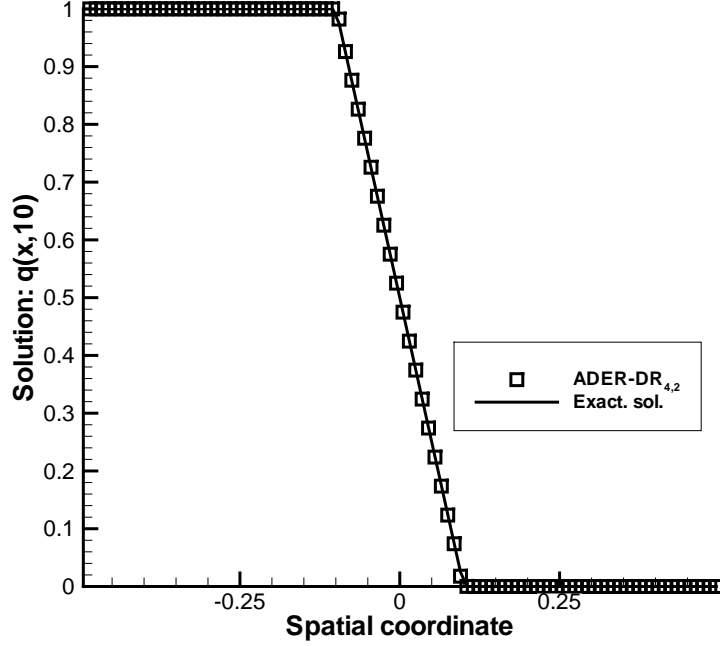


Figure 9: Solution of problem (86). Comparison of the ADER-DR_{4,2} solution (symbols) with the exact solution (line).

finite speed of propagation is that it represents the limiting case of a hyperbolic system with relaxation. The exact solution to the problem (86) is

$$q(x, t) = \begin{cases} 1 & \text{if } x < -\sqrt{\rho t} , \\ \frac{1}{2} \left(1 - \frac{x}{\sqrt{\rho t}} \right) & \text{if } x \in [-\sqrt{\rho t}, \sqrt{\rho t}] , \\ 0 & \text{if } x > \sqrt{\rho t} . \end{cases} \quad (87)$$

We have solved the problem using the numerical schemes described in the previous sections, using as speed of propagation $\rho = 10^{-3}$. Regarding the discretization in space, we have used 100 cells in the spatial domain $(-0.5, 0.5)$, so that $\Delta x = 0.01$. The diffusion parameter used is $d = 0.5$. To calculate the size of the time step we use the formula $\Delta t = \frac{d\Delta x^2}{\alpha_{max}}$, where $\alpha_{max} = \frac{1}{4}$ is the maximum value of the diffusion coefficient in the domain.

Figure 9 shows results at the output time $t = 10$ using the scheme *ADER-DR*_{4,2}, where for comparison we also show the analytical solution (full line).

As a second example we take the non-linear inhomogeneous problem

$$\left. \begin{aligned} \partial_t q(x, t) &= \partial_x (q(x, t) \partial_x q(x, t)) - q(x, t) + (2 - 8x^2) e^{-2(x^2+t)} , x \in (-10, 10) , \\ q(x, 0) &= e^{-x^2} . \end{aligned} \right\} \quad (88)$$

This problem may represent, for instance, filtration in porous media, with a reaction term given by $-q(x, t)$ and a Gaussian source, time and space dependent. The exact solution of problem (88) is

$$q(x, t) = e^{-(x^2+t)} . \quad (89)$$

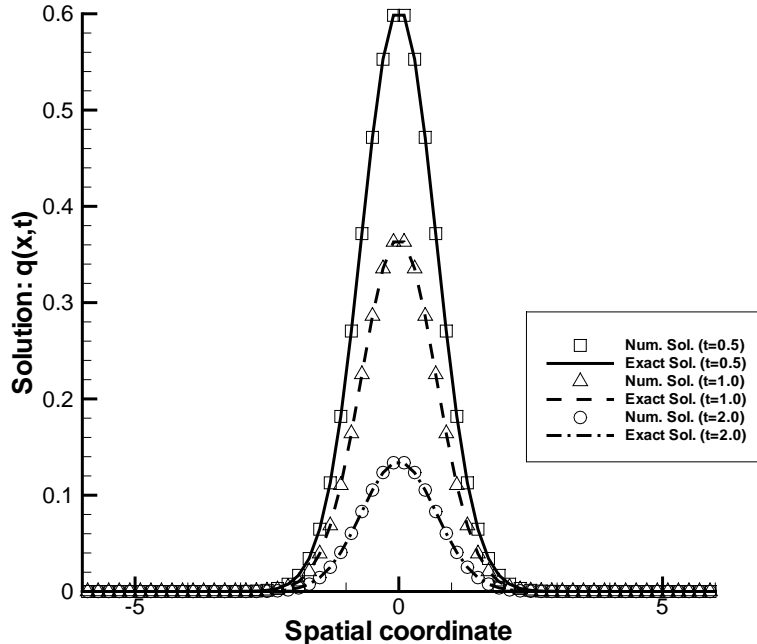


Figure 10: Solution of problem (88). Comparison of numerical solutions for several output times (symbols) with the corresponding exact solutions (line).

Results using one of the schemes described in this paper ($ADER-DR_{4,2}$) are shown in Figure 10, comparing the numerical solution with the exact solution. We have used 100 cells in the domain $(-10, 10)$. The diffusion coefficient used is $d = 0.5$. The time step is calculated according to the formula $\Delta t = \frac{d\Delta x^2}{\alpha_{max}}$, where α_{max} is the largest diffusion coefficient in the domain at any given time level. For this example, we have also calculated the convergence rates. The results obtained are shown in Table 8, for the output time $t = 0.5$.

8 Summary and Conclusions

We have constructed very-high order finite volume schemes of the Godunov type for solving non-linear diffusion-reaction parabolic equations, following the ADER approach. In our first attempt, following the Godunov approach to the letter, we found the approach to be too restrictive. A re-interpretation of the approach following the WAF framework [36], [10] is more productive, reproducing the well-known FTCS finite difference scheme, in a finite volume setting.

Another approach to generalize Godunov's method for diffusion-reaction equations is provided by the ADER methodology, in which high-order Riemann problems are solved to find numerical fluxes. We proposed methods for solving this high-order Riemann problem for non-linear diffusion-reaction equations. The initial conditions for these high-order Riemann problems are provided by a modified ENO approach; the modification requires restrictions on the length of the stencils, based on accuracy and stability considerations. Then ADER schemes of up to 10-th order of accuracy in space and time are implemented and systematically assessed, with particular attention to their convergence rates. Two numerical examples have also been presented, for which numerical results are compared against analytical solutions.

Acknowledgements. The research leading to this paper has been performed during the stay of the second author at the University of Trento, Italy, on sabbatical leave from Universidad

Politécnica de Madrid, Spain, whose support is gratefully acknowledged. Both authors thank Cedric Enaux for suggesting the first numerical problem of section 7 and for providing the analytical solution. The authors also thank Claus-Dieter Munz, Michael Dumbser, Vladimir Titarev and Carlos Conde for useful discussions on the subject.

References

- [1] T. Arbogast, M. F. Wheeler and N.-Y. Zhang. A nonlinear mixed finite element method for a degenerate parabolic equation arising in flow in porous media. *SIAM J. Numer. Anal.* 33 (4) (1996) 1669–1687.
- [2] D. N. Arnold. An interior penalty finite element method with discontinuous elements. *SIAM J. Numer. Anal.* 19 (4) (1982) 742–760.
- [3] D. G. Aronson. The porous media equation. *Lecture Notes in Mathematics* 1224, Springer-Verlag Berlin/New York, 1985.
- [4] D. G. Aronson and H.F. Weinberger. Nonlinear diffusion in population genetics, combustion and nerve pulse propagation. *Lecture Notes in Mathematics*, 1975.
- [5] D. A. Barry, J. Y. Parlange, G. C. Sander and M. Sivaplan. A class of exact solutions for Richards’ equation. *J. Hyd.* 142 (1993) 29–46.
- [6] M. Ben-Artzi and J. A. Falcovitz. A second order Godunov-type scheme for compressible fluid dynamics. *J. Comput. Phys.* 55 (1984) 1–32.
- [7] L. Bergamaschi and M. Putti. Mixed finite elements and Newton-type linearizations for the solution of Richards’ equation. *Int. J. Num. Meth. Eng.* 45 (8) (1999) 1025–1046.
- [8] J. G. Berryman and C. J. Holland. Nonlinear diffusion problems arising in plasma physics. *Phys. Rev. Lett.* 40 (26) (1978) 1720–1722.
- [9] M. Bertsch. Asymptotic behavior of solutions of a nonlinear diffusion equation. *SIAM J. Appl. Math.* 42 (1) (1982) 66–76.
- [10] S. J. Billett and E. F. Toro. On WAF-Type Schemes for Multi-Dimensional Hyperbolic Conservation Laws. *J. of Comput. Phys.*, Vol. 130, pp 1-24, 1997.
- [11] J. A. Carrillo, M. P. Gualdani and G. Toscani. Finite speed of propagation in porous media by mass transportation methods. *CR Acad. Sci. Paris, Ser. I*, (336) (2003).
- [12] P. Colella and P. Woodward. The piecewise parabolic method (PPM) for gas-dynamical simulations. *J. Comp. Phys.* 54 (1984) 174–201.
- [13] M. Dumbser, M. Kaeser, V. A. Titarev and E. F. Toro. Quadrature-free non-oscillatory finite volume schemes on unstructured meshes for nonlinear hyperbolic systems. *J. Comput Phys.* Accepted.
- [14] K. Eriksson and C. Johnson. Adaptive Finite Element methods for parabolic problems IV: Nonlinear Problems. *SIAM J. Numer. Anal.* 32 (6) (1995) 1729–1749.
- [15] K. Eriksson, D. Estep, P. Hansbo and C. Johnson. *Computational differential equations*, Cambridge University Press, 1996.
- [16] R. Eymard, M. Gutnic and D. Hilhorst. The finite volume method for Richards’ equation. *Comput. Geosc.* 3 (3-4) (1999) 259–294.

- [17] R. Eymard, T. Gallouet and R. Herbin. Finite volume methods. In: P. G.Ciarlet and J. L. Lions (Eds.). Handbook of Numerical Analysis 7 (2000) 713–1020.
- [18] G. Gassner, F. Loercher and C.-D. Munz. A contribution to the construction of diffusion fluxes for finite volume and discontinuous Galerkin schemes. J. Comput. Phys. (2006). doi:10.1016/j.jcp.2006.11.004.
- [19] S. K. Godunov. A finite difference method for the computation of discontinuous solutions of the equations of fluid dynamics. Mat. Sbornik 47 (1959) 357–393.
- [20] A. Harten, B. Engquist, S. Osher and S. Chakravarthy. Uniformly high order accurate essentially non-oscillatory schemes III. J. Comput. Phys. 71 (1987) 231–303.
- [21] J. Hernández. High order finite volume methods for the advection-diffusion equation. J. Numer. Meth. Eng. 53 (2002) 1211–1234.
- [22] Z. Krivá and K. Mikula. An adaptive finite volume scheme for solving nonlinear diffusion equations in image processing. J. of Visual Communication and Image representation 13 (2002) 22–35. doi:10.1006/jvci.2001.0502
- [23] P. Kumar. Layer averaged Richards’ equation with lateral flows. Adv. Water Resour. 27 (2004) 521–533.
- [24] I. Lakkis and A. F. Ghoniem. Axisymmetric vortex method for low-Mach number, diffusion-controlled combustion. J. Comput. Phys. 184 (2) 435–475. doi:10.1016/S0021-9991(02)00030-X
- [25] R. J. LeVeque. Finite volume methods for hyperbolic problems. Cambridge texts in applied mathematics. Cambridge University Press, 2002.
- [26] A. Michel. A finite volume scheme for two-phase immiscible flow in porous media, SIAM J. Num. Anal. 41 (4) (2003) 1301–1317.
- [27] K. Mikula and N. Ramarosy. Semi-implicit finite volume scheme for solving nonlinear diffusion equations in image processing. Numerische Mathematik 89 (3) (2001) 561–590. doi:10.1007/PL00005479
- [28] J. D. Murray. Mathematical Biology I&II, 3rd Ed., Springer-Verlag, New York, 2002.
- [29] W. Okrasinski , M.I. Parra and F. Cuadros. Modeling evaporation using a nonlinear diffusion equation. J. Math. Chem. 30 (2) (2001) 195–202. doi:10.1023/A:1017975720418.
- [30] S. Pamuk. Solution of the porous media equation by Admonian’s decomposition method. Physics Letters A 344 (2005) 184–188.
- [31] C. Z. Qu. Exact solutions to nonlinear diffusion equations obtained by a generalized conditional symmetry method. IMA J. App. Maths. 62 (1999) 283–302.
- [32] C. W. Shu, D. Levy and J. Yan. Local discontinuous Galerkin methods for nonlinear dispersive equations. J. Comp. Phys. 196 (2) (2004) 751–772.
- [33] V. A. Titarev and E. F. Toro. ADER:arbitrary high order Godunov approach. J. Sci. Comput. 17 (2002) 609–618.
- [34] V. A. Titarev and E. F. Toro. Analysis of ADER and ADER-WAF schemes. IMA J. Numerical Analysis (2006). doi:10.1093/imanum/drl033.
- [35] V. A. Titarev and E. F. Toro. High order ADER schemes for scalar advection-diffusion-reaction equations. J. Computational Fluid Dynamics, (12) (2003) 1–6.

- [36] E. F. Toro. A Weighted Average Flux Method for Hyperbolic Conservation Laws. *Proc. Roy. Soc. London A* 423 (1989) 401–418.
- [37] E. F. Toro and V. A. Titarev. Solution of the generalised Riemann for advection-reaction equations, *Proc. Roy. Soc. London* 458 (2018) (2002) 271–281.
- [38] E. F. Toro and V. A. Titarev. Derivative Riemann solvers for systems of conservation laws an ADER methods. *J. Comput. Phys.* 212 (2006) 150–165. doi:10.1016/j.jcp.2005.06.018.
- [39] E. F. Toro. Riemann solvers and numerical methods for fluid dynamics. A practical introduction, 2nd ed., Springer-Verlag, 1999.
- [40] E. F. Toro, R. C. Millington and L. A. M. Nejad. Towards very high order Godunov schemes. In E. F. Toro (Ed.), *Godunov Methods: Theory and applications*,. Kluwer/Plenum Academic Publishers, (2001) 907–940.
- [41] M. Th. van Genuchten and P. J. Wierenga. Mass transfer studies in sorbing porous media I. Analytical solutions. *J. Soil Sci. Soc. of America* 40 (4) (1976).
- [42] B. van Leer and S. Nomura. Discontinuous Galerkin for diffusion. In 17th AIAA Computational Fluids Dynamics Conference (June 6-9 2005), AIAA-2005-5108.
- [43] J. L. Vázquez. Asymptotic behaviour of the porous media equation posed in the whole space. *J. Evol. Equ.* 3 (2003) 67–118.
- [44] J. L. Vázquez. The porous medium equation. Mathematical theory. Oxford mathematical monographs, 2006.
- [45] H. Wilhelmsson. Simultaneous diffusion and reaction processes in plasma dynamics. *Phys. Rev. A* 38 (1988) 1482–1489.
- [46] E. C. Zachmanoglou and D. W. Thoe. *Introduction to partial differential equations*. Dover Publications, Inc. New York, 1986.
- [47] Y. B. Zel’dovich, G. I. Barenblatt, V. B. Libovich and G. M. Makhviladze. *The mathematical theory of combustion and explosions*. Consultants Bureau, New York 1985.